Sensitivity of Air–Sea Fluxes to SST Perturbations

ILYA RIVIN* AND ELI TZIPERMAN

Environmental Sciences, Weizmann Institute of Science, Rehovot, Israel

(Manuscript received 10 May 1996, in final form 3 October 1996)

ABSTRACT

The sensitivity of long-term averaged air–sea fluxes calculated by a 3D atmospheric general circulation model to SST perturbations of an idealized spatial structure is investigated as a function of the SST perturbation amplitude, spatial scale, latitude, and season. This sensitivity is a dominant, yet largely unknown, parameter determining the stability and variability behavior of ocean-only model studies of decadal climate variability.

The air–sea heat-flux anomaly induced by the SST perturbation varies linearly with respect to the SST perturbation amplitude in a wide range of perturbation amplitudes (±3°C). The implied restoring time of the nonglobal SST perturbations by the air–sea fluxes is found to vary from 1.5 to 3 months (for a 50-m oceanic mixed layer and perturbation scale of less than 3.4×10^6 m) depending on the spatial scale, latitude, and season of the SST anomaly. The calculated restoring time for global perturbation is of the order of two years, and the latent heat flux is found to be the air–sea heat-flux component most sensitive to SST perturbations. Both longwave and shortwave radiative fluxes are much less sensitive than latent and sensible turbulent fluxes for nonglobal SST anomalies.

The restoring time is found to be significantly longer for large-scale anomalies than for the small-scale ones, because of the dominant effect of the heat advection by wind over small perturbations. No significant difference is found between the restoring times for SST perturbations in midlatitudes and in the Tropics. SST perturbations are dissipated faster by the air–sea fluxes during the winter than during the summer. The air–sea freshwater flux anomaly is also found to strongly depend on the SST perturbation amplitude, and to vary almost linearly with the SST perturbation in the midlatitudes, but in a nonlinear way in the Tropics. The possible model dependence of the calculated restoring times is analyzed.

1. Introduction

The atmosphere and ocean are the central components of the climate system responsible for decadal and interdecadal climate variability. Most studies of climate stability and variability on timescales of a decade or longer have been performed using ocean-only models, often using the so-called mixed boundary conditions (e.g., Bryan 1986; Marotzke 1989; Mikolajewicz and Maier-Reimer 1990; Weaver et al. 1991; Winton and Sarachik 1993; Moore and Reason 1993; Maier-Reimer et al. 1993; Power et al. 1994; Weaver and Hughes 1994; Weisse et al. 1994; Cai and Godfrey 1995; Yin and Sarachik 1995; Chen and Ghil 1995). In mixed boundary conditions, the air–sea freshwater flux is assumed to be time independent and the air–sea heat flux is proportional to the difference between the SST and a prescribed near-surface atmospheric temperature.

The proportionality coefficient in the heat-flux formulation is the inverse of the characteristic time by which sea surface temperature (SST) perturbations are dissipated, often termed ''atmospheric restoring time.'' This restoring time depends, of course, on the assumed depth of the oceanic mixed layer. It is understood now that important climate feedbacks are missed by treating the freshwater flux as constant (Marotzke 1994). Recent ocean-only model studies have also demonstrated that the stability and variability of the oceanic thermohaline circulation (THC) are extremely sensitive to the value of the restoring time in the heat-flux formulation (Zhang et al. 1993; Power and Kleeman 1994; Rahmstorf and Willebrand 1995; Mikolajewicz and Maier-Reimer 1994). Furthermore, the value of this parameter is expected to depend on the scale of the SST perturbation (Willebrand 1993; Rahmstorf and Willebrand 1995; Power et al. 1995; Capotondi and Saravanan 1996). Phillips and Semptner (1984) suggested that the rate of the atmospheric dissipation of an SST anomaly should also depend on the season and latitude. A better and more quantitative knowledge of the sensitivity of air–sea fluxes to SST perturbations is clearly needed for model studies of climate stability and variability.

The use of restoring boundary conditions in ocean-only models implies a linear response of the air–sea

* Permanent affiliation: St. Petersburg Branch, P. P. Shirshov Institute of Oceanology, St. Petersburg, Russia.

Corresponding author address: Dr. Eli Tziperman, Environmental Sciences, Weizmann Institute of Science, Rehovot 76100, Israel.
E-mail: rivin@io.spb.su or citziper@weizmann.weizmann.ac.il

fluxes to SST perturbations. Such a linear response is plausible for small amplitude SST anomalies (Bretherton 1982), but not necessarily for SST perturbations of a few degrees occurring in natural decadal climate variability. A nonlinear dependence of the air–sea flux on the SST is of interest as it may lead to self-sustained thermohaline variability (Rivin and Tziperman 1997).

In this study we use a 3D atmospheric general circulation model (AGCM) to address two main questions crucial to our understanding and modeling of decadal climate variability. First, is the air–sea flux response to SST perturbations linear? Second, what is the dependence of the sensitivity of the air–sea fluxes to SST perturbations on the scale, latitude, season, and amplitude of the SST perturbations? We examine the local response of the atmospheric fluxes to a SST perturbation. Nonlocal response, such as remote changes in the air–sea freshwater flux due to changes in the meridional moisture transport in the atmosphere (Nakamura et al. 1994) is also important, but is not considered here.

Several of the above issues concerning the response of air–sea fluxes to SST perturbations were examined by Power et al. (1995) using both an AGCM and a simple atmospheric model. They analyze the linearity of the atmospheric response to SST perturbations in the North Atlantic, using two anomalous experiments with ordinary and doubled perturbation amplitude. Also, Power et al. (1995) touched upon the issue of the scale dependence of the response, comparing the atmospheric response to the SST perturbation over the North Atlantic with the response to the global perturbation in the simple atmospheric model. In this paper we present a detailed analysis of these two issues. We use the R15 version of the 3D primitive equation NCAR CCM1 global atmospheric model (see the appendix for brief description of the air–sea flux parameterization in this model). This model is especially relevant to our purpose as it is similar to the AGCMs used in coupled model studies of climate variability (e.g., Washington and Meehl 1989; Manabe et al. 1991; Delworth et al. 1993).

This study uses an idealized spatial structure of the SST perturbations that does not follow the SST perturbations induced in observed decadal variability. This is done in order to allow a simple framework for examining the dependence of the atmospheric restoring on the size, latitude, season, and amplitude of these SST perturbations. This approach, while having it advantages, such as avoiding complications due to complex spatial structure and due to the proximity of SST perturbations to landmasses, must clearly be complemented by studies such as of Power et al. (1995), who examined more realistic perturbation patterns, though in a less systematic way than could be done in the present study due to the simple SST patterns used. In addition, because our motivation in choosing the idealized SST perturbation locations is that of THC stability, most of our SST perturbations are chosen to be at midlatitudes. ENSO-related tropical SST perturbation are therefore not addressed here at all, and they may be expected to induce a significantly different atmospheric response than the perturbations considered here.

The outline of this paper is as follows. The numerical experiments are described in section 2. In section 3 we describe the dependence of the air–sea heat flux on SST perturbations of different amplitude, position, spatial scale, and season, and in section 4 we analyze the response of the air–sea freshwater flux. We compare our results concerning the dependence of the atmospheric response on the spatial scale of the SST perturbation with the Rahmstorf and Willebrand (1995) parameterization in section 5. The model dependence of our results is discussed in section 6 and we conclude in section 7.

2. Model runs

Because the atmospheric adjustment time is much smaller than the decadal and longer timescales of THC variability, the ocean only feels the long-term averaged atmospheric response to SST perturbations. The short-term (weeks) transient atmospheric response is therefore not of interest in the present study. Thus, for each SST perturbation considered here, the atmospheric model is run for two years until fully adjusted with the perturbed SST, and then for four to eight additional years in order to calculate the time-averaged response of the air–sea fluxes. In addition, this study concentrates on the local response of the air–sea fluxes to SST perturbations and disregards remote influences [those were investigated in numerous studies, such as Kutzbach et al. (1977), Chervin et al. (1980), Hoskins and Karoly (1981), Webster (1981), Frankingoul (1985a,b), Blackmon (1985), Lau and Nath (1990), Kushnir and Lau (1992)]. The atmospheric response to SST perturbations near continents is strongly influenced by the advection of air masses from the land and is therefore not in the local equilibrium with the SST (Seager et al. 1995), and is determined by remote processes. To avoid these complications we study the response to SST perturbations in four areas situated far from continents. We examine small-, medium-, and large-area perturbations at midlatitudes (denoted as MS, MM, ML, correspondingly), and a small-area perturbation in the Tropics (TS). All perturbations are situated in the North Pacific Ocean as shown in Fig. 1 and Table 1. The SST is uniformly perturbed in each region and the atmospheric response, averaged over the region of perturbation, is examined. The spatial structure of the atmospheric response is analyzed in section 3a.

The atmospheric response to SST perturbations is expected to vary seasonally. To examine this response in as simple a framework as possible, we use perpetual month experiments in which the solar radiation and background SST are fixed to those of a specified month for the entire duration of the model integration. Most of our experiments are carried out using a perpetual January background (experiments denoted MSjan,

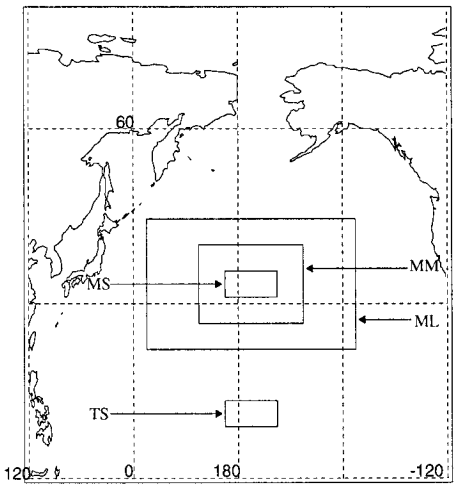

FIG. 1. Positions of the SST perturbations used in this study.

MMjan, MLjan, TSjan). In addition, in order to obtain a preliminary understanding of the seasonal dependence, two series of perpetual July experiments were carried out, for the medium-scale midlatitude perturbation (MMjul) and for a globally perturbed SST (GBjul). The idealized SST perturbation patterns used here, while clearly artificial, allow us to examine the atmospheric response for a wide range of perturbations in as simple as possible framework. Future studies will need to examine the effects of the proximity to landmasses and complex SST patterns, in addition to the many effects examined here due to amplitude, size, season, and latitude. The full list of experiments used in this study is given in Table 2.

The sensitivity of the air–sea flux to SST perturbations is most conveniently presented in terms of an atmospheric restoring time that is derived as follows. In most ocean-only studies, the air–sea heat-flux parameterization is of the form

$$Q(x, y, t) = \rho_w c_{pw} \Delta z \gamma_T (T^* - T_o), \qquad (1)$$

where Q is the air–sea heat flux, T^* is the restoring temperature, T_o is the model SST, ρ_w is the water density, $c_{pw} = 3930$ J kg^{-1} K^{-1} is the specific heat of water, Δz is the depth of the oceanic mixed layer, and γ_T is the restoring coefficient (inverse restoring time) for the temperature. Motivated by the simple restoring parameterization of air–sea heat flux, we can calculate an equivalent atmospheric restoring time for the fuller heat flux parameterization of our AGCM. Given the heat flux sensitivity to SST perturbations, $\partial Q/\partial T_o$, deduced from our atmospheric model experiments, the restoring time is

$$\tau = 1/\gamma_T = -\rho_w c_{pw} \Delta z/(\partial Q/\partial T_o). \qquad (2)$$

The mixed layer thickness in the ocean varies from ten to a few hundred meters (Gill 1982). As coarse ocean models used for climate studies often use a 50-m upper-level thickness, we use $\Delta z = 50$ m to calculate the restoring times. Physically, the restoring time represents the timescale at which the atmosphere is expected to dissipate SST perturbations over a depth of Δz.

3. Air–sea heat-flux sensitivity to SST perturbations

Let us consider first the atmospheric response to an SST perturbation of a medium scale (MM in Fig. 1), situated at midlatitudes, under perpetual January conditions (experiment MMjan, Table 2). The squares in Fig. 2a display the perturbation air–sea heat flux averaged over the perturbation area as a function of the perturbation SST amplitude. A positive heat-flux anomaly in these plots indicates that the ocean is gaining more heat. The figure clearly demonstrates that the net air–sea heat-flux anomaly, as well as its components, depend linearly on the SST perturbation amplitude in a wide range of perturbation from -3°C to $+3$°C. This range is larger than present-day decadal SST variability in most off-equatorial regions of the World Ocean (Peixoto and Oort 1992). Note that the scatter around the line fit is very small. Each point in Fig. 2 is obtained by averaging over four years of model runs. Figure 2F shows the error bars based on the scatter of these four-yearly averages, demonstrating that the linear fit is indeed significant. This robust linear behavior is somewhat surprising given the nonlinearity of the atmospheric model and of the air–sea flux parameterization (see appendix). We shall begin our discussion of the MMjan experiments by trying to explain this linearity, starting from the linear behavior of the turbulent (latent and sensible) heat flux components.

Sensible and latent air–sea heat fluxes in atmospheric models are usually calculated by bulk formulas such as (A3) and (A4) in the appendix. These fluxes depend on the prognostic air temperature T_h, the specific humidity q_h, and the wind velocity V_h, all evaluated at the lowest atmospheric level. Changes in the averaged wind ve-

TABLE 1. The location of SST perturbations used in this study. Here, N is the number of horizontal grid points per perturbation, the area is in 10^{12} m^2, and E–W is the east–west extent of the perturbation (in 10^6 m).

Perturbation	Position	N	Area	E–W
MS	31.1°–35.6°N, 176.3°E–168.8°W	4	1.43	0.86
TS	8.9°–13.3°N, 176.3°E–168.8°W	4	1.65	0.99
MM	26.7°–40.0°N, 168.8°E–161.3°W	16	5.70	1.71
ML	22.2°–44.4°N, 153.6°E–146.3°W	48	17.00	3.40
GB	All open-ocean points	1045	204.75	—

TABLE 2. Summary of model runs used in this study. Here, + denotes a 6-yr model run with the results averaged from the third to the sixth year, and ◇ denotes a 10-yr model run with the results averaged from the third to the tenth year.

	ΔSST (K)												
Perturbation	−3	−2	−1.5	−1	−0.5	−0.25	0.25	0.5	1	1.5	2	2.5	3
MSjan	+	+	+	+	+	◇	◇	+	+	+	+		+
MMjan	+	+		+					+		+		+
MLjan	+	+		◇					◇		+		+
TSjan	◇	◇		◇					+		+	+	+
MMjul	+	+		+					+		+		+
GBjul	+	+		+					+		+		+

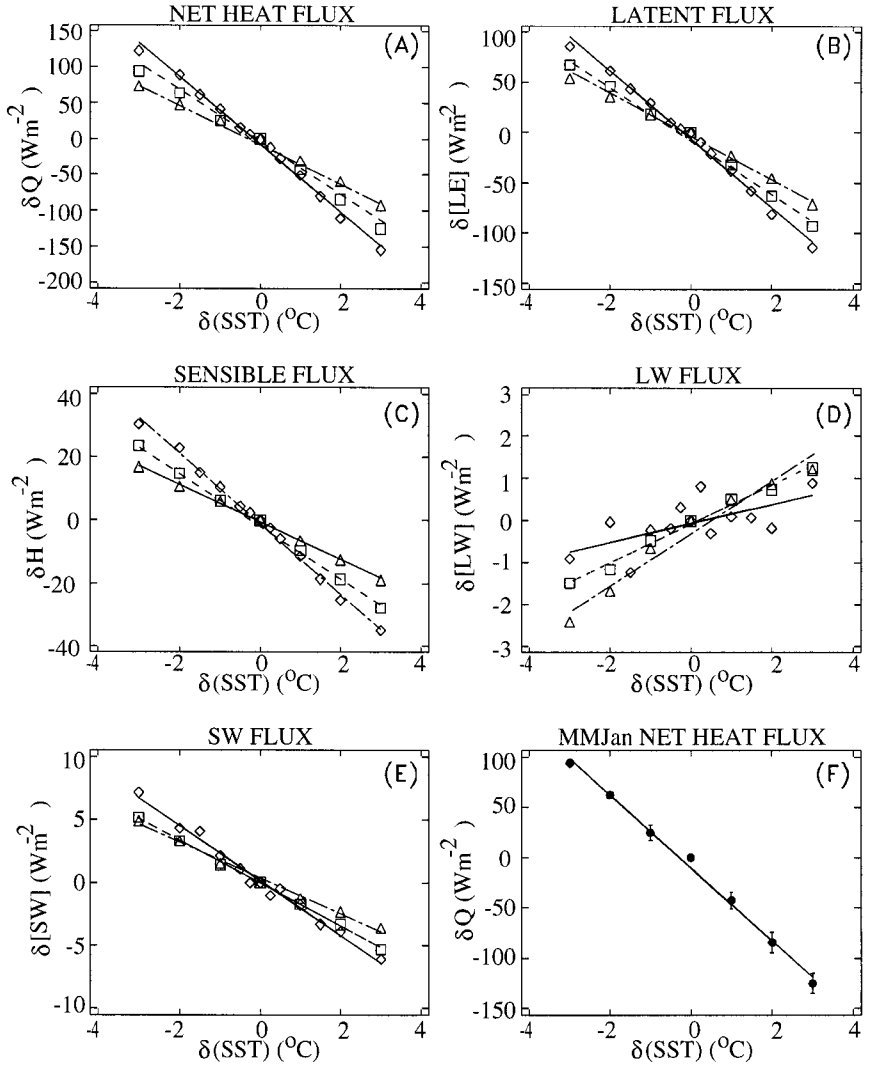

FIG. 2. Air–sea heat-flux anomalies (in W m^{-2}) vs SST perturbation amplitude, and the best-fit lines, for the MSjan (diamonds, solid line), MMjan (squares, dash), and MLjan (triangles, dash–dot) SST anomalies. The fluxes are averaged over the region of the SST perturbation. (a) Net air–sea heat flux. (b) Latent air–sea heat flux. (c) Sensible air–sea heat flux. (d) Longwave air–sea heat flux. (e) Shortwave air–sea heat flux. (f) Net air–sea heat-flux anomaly for the MMjan SST perturbation. Dots denote the 4-yr averaged fluxes. The error bars are based on the variation within the 4-yearly averages used to calculate the 4-yr mean.

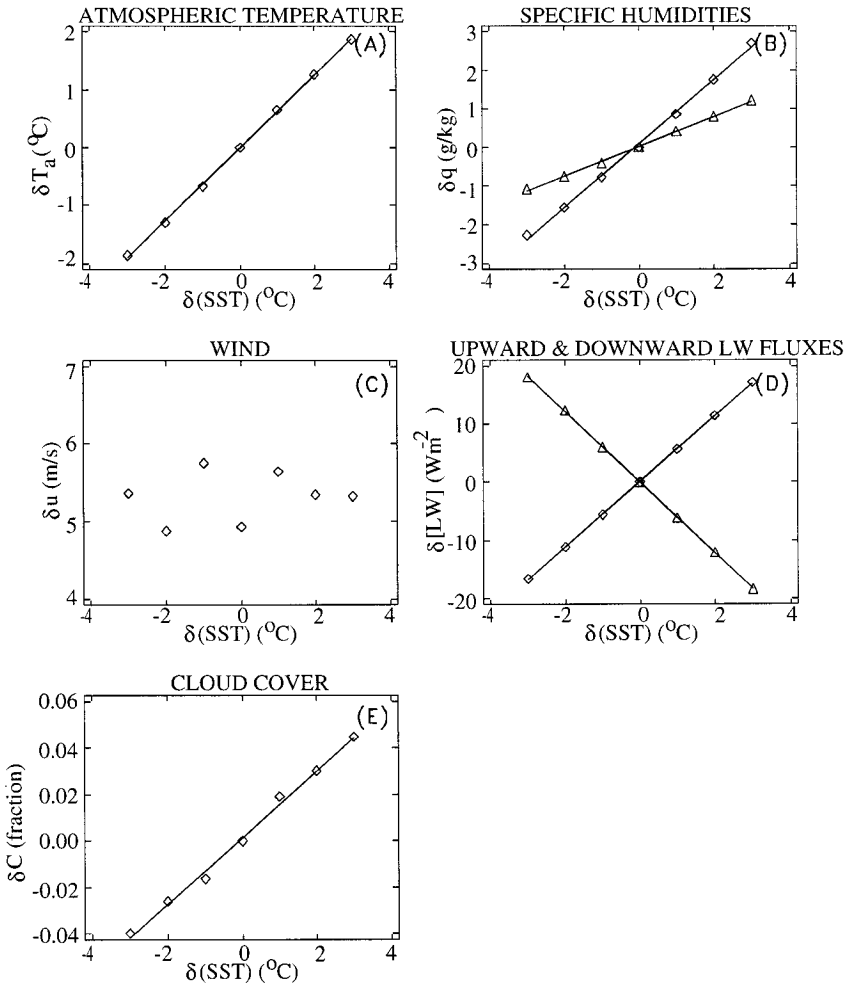

FIG. 3. Atmospheric variables used to calculate the air–sea heat fluxes, averaged over the region of SST anomaly, vs the SST perturbation anomaly for the MMjan experiments. (a) Atmospheric temperature anomaly at the lowest level (in °C). (b) Specific humidity anomaly at the lowest atmospheric model level (diamonds) and saturation humidity anomaly at the surface anomaly (triangles) (in g kg^{-1}). (c) Wind velocity at the lowest level (in m s^{-1}). (d) Upward (diamonds) and downward (triangles) LW fluxes at the surface anomaly (in W m^{-2}). (e) Cloud cover anomaly (in fractions of unity).

locity due to the SST perturbation are of the order of 20% and are random as seen in Fig. 3c (as a caveat, we note that these wind changes may be especially sensitive to the idealized SST patterns used here). While the changes in atmospheric temperature are small compared to the temperature as measured in kelvins, the changes in the difference between the SST and the lowest-level atmospheric temperature are of the order of the difference itself. Both the wind and the drag coefficient (C_H) that appear in the air–sea flux parameterizations vary with the SST. The drag coefficient is a function of the bulk Richardson number in this model, and, in addition, the functional form of its dependence on the atmospheric quantities varies depending on the lower atmospheric static stability (Williamson et al. 1987). However, as evident from the linear dependence of the air–sea flux anomalies on the SST perturbation, the linear changes to the air–sea temperature difference clearly dominate the possible nonlinearities due to the drag coefficient and wind speed. Similarly, changes to the humidity differences in the equation for the latent heat dominate the response of this flux. Hence, the response of the turbulent air–sea fluxes to SST perturbations is mainly determined by the response of the temperature and the humidity at the lowest atmospheric level [the former for the sensible flux and the latter for the latent flux, see (A3) and (A4)].

As seen in Fig. 3a, the anomaly in the lowest-level atmospheric temperature T_h in the MMjan experiments is a linear function of the SST for perturbations from -3°C to $+3$°C. The sensible air–sea heat-flux anomaly is a linear function of T_h (A3), and since changes in the wind speed are small, the sensible heat flux depends linearly on the SST perturbation. In reality, the drag

TABLE 3. The sensitivity of the various air–sea flux components to the different SST perturbations considered in this study. The sensitivity is presented both in terms of restoring times for a 50-m-deep mixed layer (in days, left of slash), and as $|\Delta\psi/\Delta(\mathrm{SST})|$, where ψ is one of the air–sea flux components, in units of W m^{-2} (°C)$^{-1}$ (right of slash). The different columns show the sensitivity of the net (Q), latent (LE), sensible (H), net shortwave (SW), and upward ([LW]↑) and downward ([LW]↓) longwave (LW) air–sea heat-flux components.

Perturb.	Q	LE	H	SW	LW	[LW]↑	[LW]↓
MSjan	48/47	67/34	203/11	1041/2	10 127/0.2	404/6	388/6
MMjan	62/36	85/27	270/8	1330/2	4899/0.5	404/6	373/6
MLjan	83/27	110/21	384/6	1611/1	3721/0.6	405/6	366/6
TSjan	44/51	56/41	318/7	401/6	898/2	369/6	261/9
MMjul	91/25	130/17	496/5	554/4	2029/1	404/6	337/7
GBjul	614/4	475/5	33 961/0.1	35 815/0.1	1882/1	407/6	334/7

coefficient may depend more explicitly on the static stability, and the wind anomaly on the SST perturbation structure, which is taken uniform here. Together, these dependencies may modify somewhat the robustly linear response we see here.

The latent air–sea heat flux is a function of the difference between the saturation specific humidity at the sea surface, q_m, and the specific humidity at the lowest atmospheric model level, q_h [A4]. Figure 3b shows that the changes in both quantities are linear with respect to the SST perturbations. By the Clausius–Clapeyron equation, the saturation specific humidity $q_m(T)$ is proportional to $\exp(-AT)$ where $A = \text{const} > 0$. An expansion of the difference $q_m(\bar{T}_o + T'_o) - q_m(\bar{T}_o)$ in a Taylor series around the unperturbed SST, $\bar{T}_o$, results in a series of the form $\Sigma_{n=1}^{\infty} B_n(T'_o)^n$, with the coefficients B_n proportionally to the n's power of $1/\bar{T}_o$. Since $\bar{T}_o > 273$ and $|T'_o| \leq 3$, so that $|\bar{T}_o| \gg |T'_o|$, the linear term is dominant. Therefore, the saturation specific humidity is linear with respect to SST in the range of SST perturbations relevant to present-day climate variability. Therefore, the anomalies of the difference $q_m(T_o, p_a) - q_h$, and thus the latent air–sea heat-flux anomaly, are also linear with respect to the SST perturbation amplitude.

The linear response of the anomalies induced in the incoming shortwave (SW) solar radiation is a direct consequence of the linear response of the vertically averaged cloud cover (Fig. 3e) (which mainly results from the response of the lower-level cloudiness) and air humidity (Fig. 3b, which cause a linear response of the atmospheric absorption of the SW radiation on its way to the ocean surface. The upward longwave (LW) heat flux released by the ocean is formally proportional to the fourth power of the SST [the first term on the rhs of (A2)], but as $(\bar{T}_o + T'_o)^4 - \bar{T}_o^4 = [4\bar{T}_o^3 T'_o + 6\bar{T}_o^2(T'_o)^2 + 4\bar{T}_o(T'_o)^3 + (T'_o)^4]$ and because $\bar{T}_o$ is about two orders of magnitude larger than $|T'_o|$, it is obvious that the first term in the square brackets, linear with respect to the SST perturbation, is dominant. The downward LW air–sea radiation (Fig. 3d) is emitted mainly by atmospheric clouds and water vapor and its anomaly response is also linear due to the linear changes of the air temperature, humidity, and the cloud cover anomalies with the SST perturbation.

Let us compare the sensitivities of the different components of the air–sea heat flux, starting again with the turbulent fluxes. The restoring times (calculated for a 50-m oceanic mixed layer) for the different air–sea heat-flux components are given in Table 3. The most sensitive response is that of the latent heat flux (Fig. 2b). It is always negative since the ocean always looses heat during evaporation; the latent heat is later realized in the atmosphere during precipitation, but is not necessarily close in space or time to the region of evaporation. The latent heat-flux sensitivity is greater than that of the sensible flux sensitivity (Table 3). While both of these turbulent air–sea heat flux components depend mostly on the SST to near-surface air temperature difference, there is a major difference between them. The sensible air–sea heat flux strongly affects the local near-surface air temperature. Latent heat flux, on the other hand, does not influence air temperature directly, and in the presence of strong horizontal advection (which leads to the precipitation of the evaporated water in a remote region) may not influence it at all.

The restoring times for the longwave (Fig. 2d) and the shortwave radiative fluxes (Fig. 2e) are much longer than for the turbulent (latent and sensible) heat fluxes. The longwave radiative air–sea heat flux is the difference between downward longwave radiation emitted by the atmosphere and the upward longwave emission of the ocean. While both of these components are quite sensitive to SST perturbations (Table 3), their sum changes very little with the SST (Figs. 2d and 3d). Consequently, the restoring time for the net LW air–sea heat flux is about an order of magnitude longer than for each of its components (Table 3).

The longwave radiation emission from the surface (Fig. 3d) increases as the fourth power of the SST, according to the Stephan–Boltzmann formula [second term on the rhs of (A2)]. The downward LW atmospheric radiation (Fig. 3d) is the sum of cloud emission and clear-sky radiation. The downward radiation from clouds increases with the SST due to the increase of both cloudiness and temperature of the cloud bottom. In addition, the increase of atmospheric humidity leads to the growth of clear-sky LW radiation, but simultaneously this process causes an increased absorption by the clear-sky humidity of the downward radiation from clouds. The sum of all of these processes is the increase of downward LW radiation seen in Fig. 3d.

The above analysis is of the atmospheric response above the SST perturbation area. Clearly, the dependence of the air–sea fluxes on the local SST perturbation outside the perturbation area may be both nonrestoring and nonlinear because the local SST perturbation is zero while the atmospheric response may be nonvanishing due to wind advection effects (Power et al. 1995). We center our analysis here, however, on the local response above the perturbation area, which is also the dominant atmospheric response.

a. Heat-flux sensitivity as function of the spatial scale of the SST perturbation

It is generally believed that the sensitivity of the air–sea heat flux to SST perturbations as expressed in the atmospheric restoring time should depend on the spatial scale of the SST anomaly (Frankingoul 1985a; Willebrand 1993; Marotzke 1994; Rahmstorf and Willebrand 1995; Kleeman and Power 1995; Power et al. 1995). To explore this scale dependence, we compare the air–sea flux sensitivity to small-, medium-, and large-scale SST perturbations at midlatitudes (the MSjan, MMjan, MLjan experiments, Fig. 2).

As shown in Fig. 2, the sensitivity of the net air–sea heat flux decreases for larger spatial scales of the SST perturbations (Table 3). The restoring time is 48 days for the smallest perturbation (MSjan), 62 days for the mediun-scale perturbation (MMjan), and 83 days for the largest-scale (MLjan) perturbation. This dependence on the scale of the perturbation is because for the small-area perturbations the perturbation heat flux can be advected away from the perturbation area while for the large-area perturbations the advection could not efficiently remove the heat from the entire perturbation area. Therefore, for large-scale perturbations, the local atmospheric temperature above the SST perturbation is more influenced by the SST anomaly and closely follows the changes in the SST. Consequently, the air–sea temperature difference does not change significantly with the SST perturbation amplitude for large-scale SST perturbations. The turbulent air–sea heat fluxes that depend on this temperature difference are thus less sensitive to larger-scale SST perturbations (Table 3).

Let us briefly consider the spatial structure of the atmospheric response, for the +3 K large-scale SST perturbation (MLjan, Fig. 4). The heat-flux anomaly is negative (cooling the ocean) due to the increased SST and is clearly not uniform. Due to the advection by wind, the air–sea heat-flux anomaly reaches a maximum negative value at the western boundary of the SST anomaly area. The positive maximum in heat flux to the south of the SST perturbation is caused by the advection of heat and mostly moisture from the region of perturbation by the northeast trade winds (Fig. 4e), causing an increase of air temperature (not shown) and humidity (Fig. 4c) to the south of the SST perturbation. The SST in this area is not perturbed in our experiments, so due to (A3) and (A4) the air–sea sensible (not shown) and latent (Fig. 4b) fluxes increase, with the latter being the major contributor to the total air–sea heat-flux response. The wind to the north of the perturbations increases more than to the south of the perturbation (Fig. 4d), largely because the geostrophic wind increase with the north–south temperature gradient is larger at the north due to the larger Coriolis acceleration there.

To extend our investigation of scale dependence of the atmospheric response, we have also carried out an experiment in which the SST is perturbed globally (GBjul, Table 3). The restoring time for the global perturbation is of the order of 2 yr, much longer than for the local SST anomalies. As in the cases of the smaller-scale SST anomalies, the latent heat flux is the most sensitive air–sea heat flux component, and it dominates the atmospheric response. This implies, of course, that there is a net evaporation over the global ocean, compensated by precipitation over land. The next most sensitive component is the LW flux, with the restoring time about three times longer than the restoring time for the latent flux. Both the latent heat and the LW radiation anomalies are robustly linear with the SST perturbation amplitude for the global perturbation as for the smaller-scale midlatitude perturbations discussed above. The sensitivities of the sensible and SW fluxes to the global perturbations are smaller by an order of magnitude than those of the dominant terms and are not completely resolved from the noise level in the 4-yr averages we use.

Power et al. (1995) compared the atmospheric restoring in the North Atlantic to the restricted and global SST perturbations in the simple atmospheric model. They conclude that the atmospheric response to the global SST perturbation is about a half of the atmospheric response to the North Atlantic only SST perturbation and there is a great deal of spatial variability of the restoring coefficients. In our experiment, the difference between basin-scale and global perturbations is much greater (see entries MLjan and GBjul in Table 3), it is partly because the area of MLjan perturbation is about a half of the area of the North Atlantic perturbation used by Power et al. (1995). In addition, the sensitivity of the air–sea fluxes in their simple atmospheric model to the global SST perturbation is two times bigger than observed in our fuller AGCM.

Our results tend to support the hypothesis of Zhang et al. (1993) that basin-scale perturbations (bigger than ML perturbation used in our study but smaller than the global one) have restoring time of the order of several hundred days. But the assumption of Schopf (1983), Zhang et al. (1993), and Marotzke (1994) that the longwave flux is the main contributor in the atmospheric response for the basin-scale and larger perturbations is not confirmed by our results. The latent flux appears to be the most sensitive component of the air–sea heat flux even for the global perturbation. Yet, the relative con-

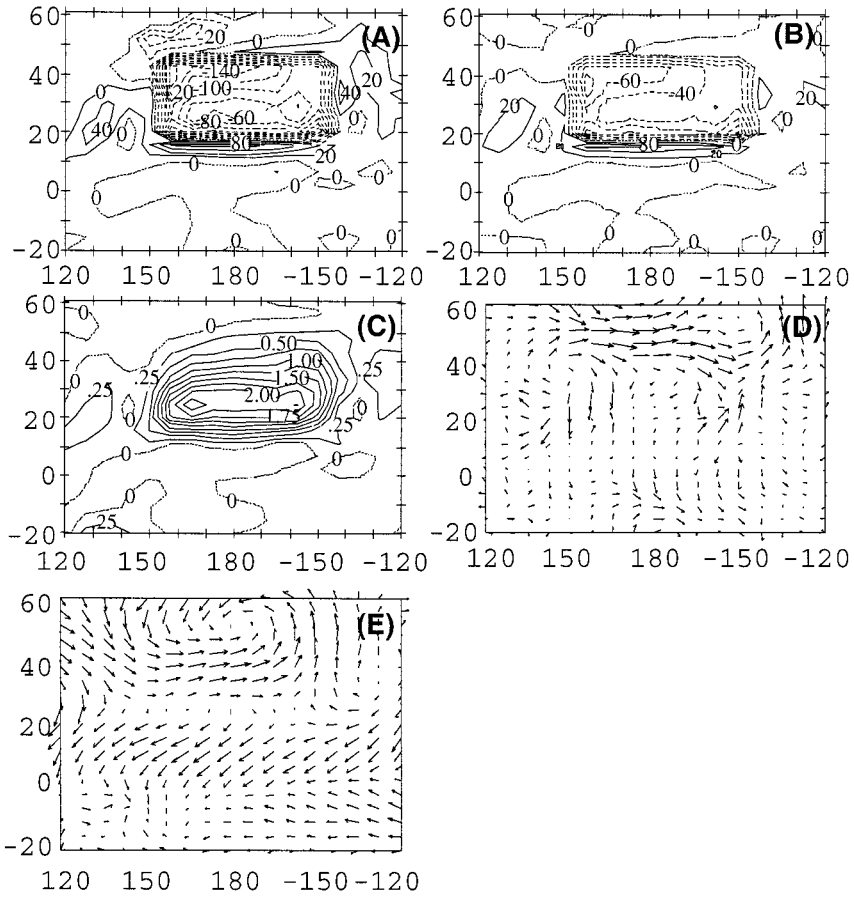

FIG. 4. The atmospheric response to the +3 K midlatitude large-area January SST anomaly (+3MLjan). (a) Air–sea heat-flux anomaly (in W m^{-2}). (b) Air–sea latent heat-flux anomaly (in W m^{-2}). (c) Absolute humidity anomaly at the lowest model level (in g kg^{-1}). (d) Wind anomaly at the lowest model level. (e) Total wind at the lowest model level in the control experiment [the vectors in subplot (d) are scaled twice as large as in subplot (e)].

tribution of the longwave flux response does increase with the increase of the SST perturbation area.

b. Heat-flux sensitivity as a function of the latitude of the SST perturbation

The atmospheric response to SST perturbations is also a function of latitude, expected to be dominated by local diabatic heating processes in the Tropics, and by advection of heat away from the region of SST anomaly at midlatitudes (Webster 1981). We analyze the latitude dependence of the atmospheric restoring of SST perturbations by comparing the response to small-scale SST perturbations in the Tropics (TSjan, curve marked by diamonds in Fig. 5) and at midlatitudes (MSjan, Fig. 2, diamonds). In both the TSjan and MSjan experiments, the SST was perturbed at four model grid points. The corresponding areas are slightly different for the two perturbations (Table 1), but as we will see, the difference in atmospheric response is more significant.

The horizontal advection of heat from the region of an SST perturbation by the wind is stronger in midlatitudes than in the Tropics, and since horizontal advection dominates the atmospheric response to small-area SST anomalies, we expected a significant difference in the atmospheric response for the MSjan and TSjan SST anomalies. Surprisingly, the restoring times are almost the same in midlatitudes (about 48 days) and in the Tropics (about 44 days). But as shown in Table 3, the restoring times for the various air–sea heat-flux components change more significantly than their sum when the perturbation is moved from midlatitudes to the Tropics.

The sensitivity of the sensible air–sea heat flux is smaller in the Tropics. Because the heat advection by wind is stronger in the midlatitudes, the air temperature above the perturbation follows the SST less closely and the sensible air–sea heat flux, being a function of the difference between the two temperatures, is more sensitive to SST perturbations (see Table 3 and the discussion of the role of horizontal advection of heat by the winds in section 3 above).

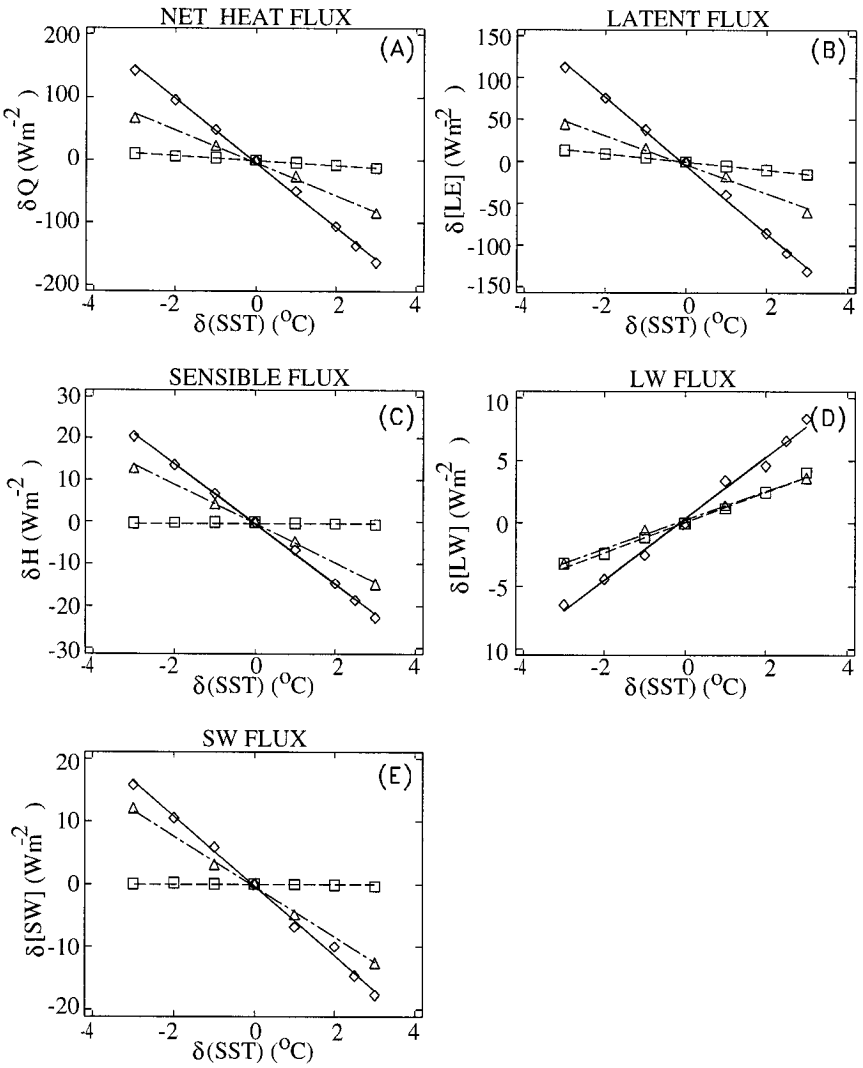

FIG. 5. Air–sea heat-flux anomalies vs SST perturbation amplitude, and the corresponding best-fit lines for the TSjan (diamonds, solid line), GBjul (squares, dash), and MMjul (triangles, dash–dot) SST anomalies (in W m^{-2}). The flux anomalies are averaged over the region of the SST perturbation. (a) Net heat flux. (b) Latent heat flux. (c) Sensible heat flux. (d) Longwave heat flux. (e) Shortwave heat flux.

In contrast to the sensible heat flux, the latent heat flux is more sensitive to the SST in the Tropics. It depends on both the saturation specific humidity at the surface, q_m, and on the specific humidity at the lowest model level, q_h [A4]. In turn, q_m is roughly an exponential function of the SST. The SST in January in the Tropics is almost 10 K higher than in midlatitudes at the same month. As a result, the slope of the exponential curves for q_m is greater in the Tropics than in midlatitudes, explaining the larger tropical sensitivity. (In the Tropics, $\partial q_m/\partial T_o = 1.3$ g kg^{-1} K^{-1} and $\partial q_h/\partial T_o = 0.5$ g kg^{-1} K^{-1}, while in midlatitudes $\partial q_m/\partial T_o = 0.8$ g kg^{-1} K^{-1} and $\partial q_h/\partial T_o = 0.3$ g kg^{-1} K^{-1}).

Note that the stronger wind advection in midlatitudes acts to make the latent heat more sensitive to the SST perturbation, for the same reason it does this for the sensible heat flux. However, the larger sensitivity of the specific humidity at the Tropics discussed above dominates this advection effect, making the latent heat flux more sensitive to the SST in the Tropics.

Thus, the different sensitivities of the air–sea flux components in the Tropics and in midlatitudes compensate, leaving the net air–sea heat-flux dependence on the SST perturbation amplitude similar.

c. *Heat-flux sensitivity as a function of the season of the SST perturbation*

To obtain a preliminary understanding of the seasonal effects on the sensitivity of air–sea fluxes to SST per-

turbations, we performed an experiment using a perpetual July model (entry MMjul in Table 3 and Fig. 5) and compared it to the perpetual January experiment (MMjan). Both the atmospheric circulation and the air–sea temperature difference in the midlatitudes are smaller in summer than in winter. Therefore, the atmosphere restores SST perturbations slower in summer than in winter. Indeed, the restoring time for the MMjul perturbation (91 days) is significantly larger than for the MMjan perturbation (62 days). The latent heat flux is again the component most sensitive to SST perturbations in the perpetual July experiments, as in the perpetual January experiments. The sensible heat-flux sensitivity is significantly reduced in the July experiment, because in July the air temperature closely follows the SST due to the weaker heat advection by the weaker summer winds.

4. Air–sea freshwater flux sensitivity to SST perturbation

In many ocean-only model studies of climate stability and variability, the air–sea freshwater flux was assumed to be independent of the SST. It is now understood that this eliminates important feedbacks between the large-scale meridional transport of moisture in the atmosphere and the THC. Nakamura et al. (1994) demonstrated that this ''eddy moisture transport − THC'' feedback may make the THC less stable.

The experiments described above can also be used to determine the dependence of the air–sea freshwater flux $[E - P]$ on the SST. Because evaporation is proportional to the air–sea latent heat flux, its sensitivity to the SST is easily deduced from the above discussion of the latent heat sensitivity. In this section we thus concentrate on the response of the precipitation and net $[E - P]$.

Consider first the midlatitude, medium-scale, perpetual January (MMjan) SST perturbations. Figure 6a shows that the air–sea freshwater flux strongly depends on the SST perturbation amplitude. For the MMjan perturbation the air–sea freshwater flux is a linear function of the SST perturbation amplitude of up to 3 K. In addition, evaporation (Fig. 6b) and both large-scale (Fig. 6d) and convective precipitation (Fig. 6e) depend linearly on SST perturbation. The reason for the linear response of evaporation on the SST anomaly was already discussed in section 3 in the context of the latent flux sensitivity. Precipitation depends mostly in the humidity in the lower troposphere (see the appendix), and its response is linear because the perturbation specific humidity appears to be a linear function of the MMjan SST perturbation amplitude (an example of the specific humidity anomaly vs SST perturbation at the lowest atmospheric level is shown in Fig. 3b). The sensitivity of evaporation to the SST, $\partial E/\partial T_o$ is about three times greater than the sensitivity of the total precipitation, $\partial P/\partial T_o$ (Figs. 6b,c and Table 4). This implies that most of the evaporation excess due to the SST anomaly is not precipitated locally (or else the evaporation and precipitation anomalies would be equal and have the same sensitivity to the SST perturbation). Rather, the strong advection in the midlatitudes carries most of the evaporated water out of the perturbation region and then precipitates remotely.

In addition, the $[E - P]$ anomaly response to SST perturbations is found to be almost linear for all three midlatitude SST perturbations (Fig. 6). Because the response of the air–sea freshwater flux at midlatitudes is mainly determined by the sensitivity of the evaporation (Table 4), the dependence of the $[E - P]$ response on the spatial scale of SST perturbations is similar to the dependence of the latent air–sea heat flux discussed above. That is, the sensitivity of the air–sea freshwater flux to SST perturbations becomes weaker for larger-scale SST perturbations (Table 4).

The dependence of the tropical air–sea freshwater flux anomalies on the SST perturbation is clearly nonlinear and its sensitivity to SST perturbations is different for positive and negative SST perturbations (Fig. 7a). This behavior of the net $[E - P]$ response is due to the nonlinear response of both the convective and the large-scale precipitations in the Tropics (Figs. 7d,e), and hence of the net precipitation anomaly (Fig. 7c). The response of the evaporation anomaly is linear with the SST perturbation amplitude for the entire range of SST perturbations used in this study (Fig. 7b). A first clue for the nonlinear behavior of the precipitation comes from noticing that for SST anomalies larger than $+2°C$, the anomalous precipitation is larger than anomalous evaporation. Thus, one suspects that some of the additional precipitation for large positive SST perturbations is supplied by the condensation of remotely evaporated water, through converging winds in the lower troposphere. This nonlocal and nonlinear effect indeed comes about due to the interaction of our SST perturbation and the nearby ITCZ. The ITCZ over the ocean is attracted to the region of maximum SST. In our experiments, a low-pressure anomaly develops over the region of the SST perturbation when this perturbation is large enough. As a result, the ITCZ shifts northward toward our tropical SST perturbation region. This results in additional precipitation over the perturbation area, and in larger sensitivity of the anomalous precipitation to the SST perturbations, as seen in Figs. 7 for positive SST anomalies. While the tropical precipitation response is clearly very interesting, it is largely outside of the focus of this paper. The motivation for this study is the study of thermohaline stability, which depends more strongly on the air–sea flux sensitivities to midlatitude SST perturbations. We thus leave a further study of the above interesting mechanisms of the nonlinear tropical precipitation response to a future study.

5. Parameterizations of local air–sea interaction in ocean-only models

Haney (1971) assumed the air–sea temperature difference to be small, so that the components of the ocean

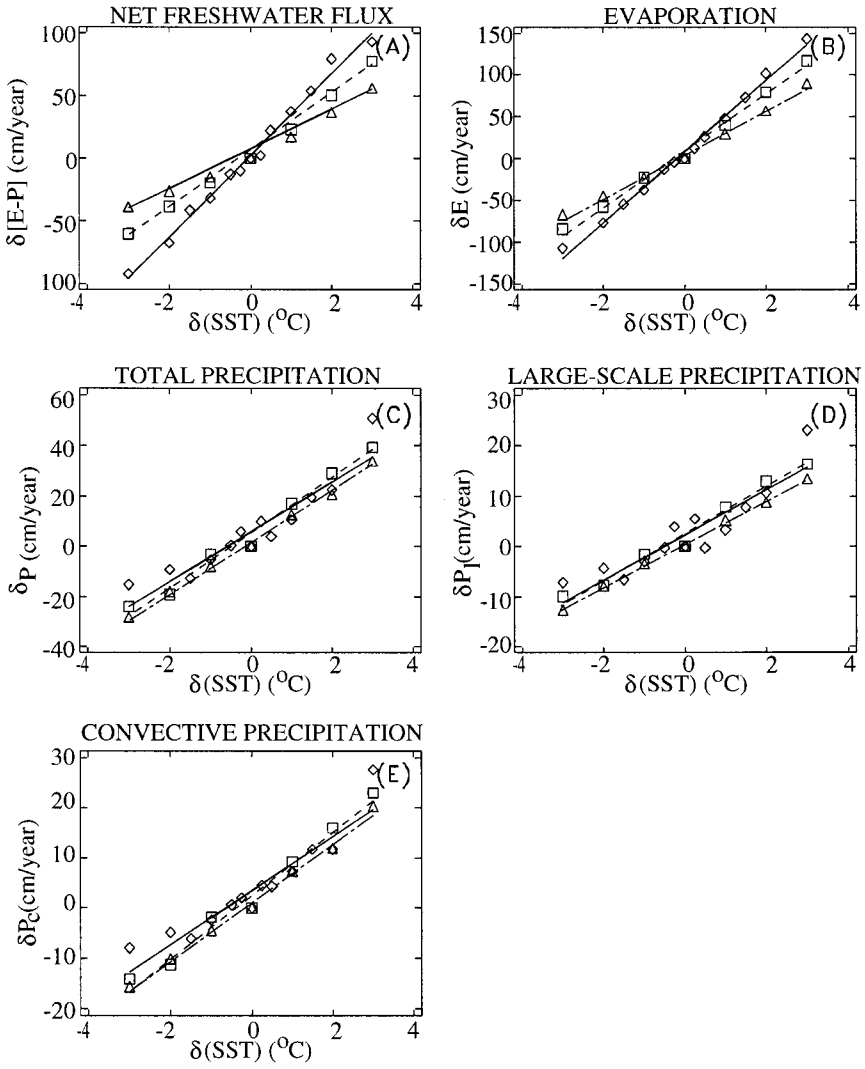

FIG. 6. Air–sea freshwater flux anomalies vs SST perturbation amplitude, and the best-fit lines, for the MSjan (diamonds, solid line), MMjan (squares, dash), and MLjan (triangles, dash–dot) SST anomalies (in cm yr^{-1}). (a) Air–sea freshwater flux anomaly. (b) Evaporation anomaly. (c) Net precipitation anomaly. (d) Large-scale precipitation anomaly. (e) Convective precipitation anomaly.

TABLE 4. The derivatives of the air–sea freshwater flux ($[E - P]$), the evaporation (E), net, large-scale (P_l), and convective (P_c) precipitation (P) with respect to the SST in 10^{-6} (kg m^{-3} s^{-1} K^{-1}).

Perturb.	$\partial[E-P]/\partial T_o$	$\partial E/\partial T_o$	$\partial P/\partial T_o$	$\partial P_l/\partial T_o$	$\partial P_c/\partial T_o$
MLjan	5.0	8.2	3.2	1.4	1.7
MMjan	7.2	10.6	3.4	1.5	2.0
MSjan	10.4	13.5	3.1	1.4	1.9
TSjan*	2.6	16.2	13.6	6.8	6.7
MMjul	4.2	7.0	2.7	1.6	1.1
GBjul	0.4	1.9	1.5	1.1	0.4

* The nonlinear behavior of the precipitation with SST in this experiment prevents a clear estimate of a sensitivity. A rough line fit is used to get the above estimate.

surface energy balance equations [lhs of (A1)] could be expanded into a truncated Taylor series about the air temperature. This results in a ''restoring'' relation between the air–sea heat flux, Q, and the SST, T_o:

$$Q = \alpha(T^* - T_o), \tag{3}$$

where $\alpha = \rho_w c_{pw} \gamma_T \Delta z$, and the parameters T^* and γ_T in (3) may vary spatially. The temperature T^* in (3) is not an atmospheric near-ocean temperature, but ''a kind of apparent atmospheric equilibrium temperature . . . which includes the effect of evaporation and radiation'' (Haney 1971).

It is sufficient to have one spatially dependent parameter, namely T^*, to fit the observed climatological mean of the air–sea heat flux data. But a realistic heat-

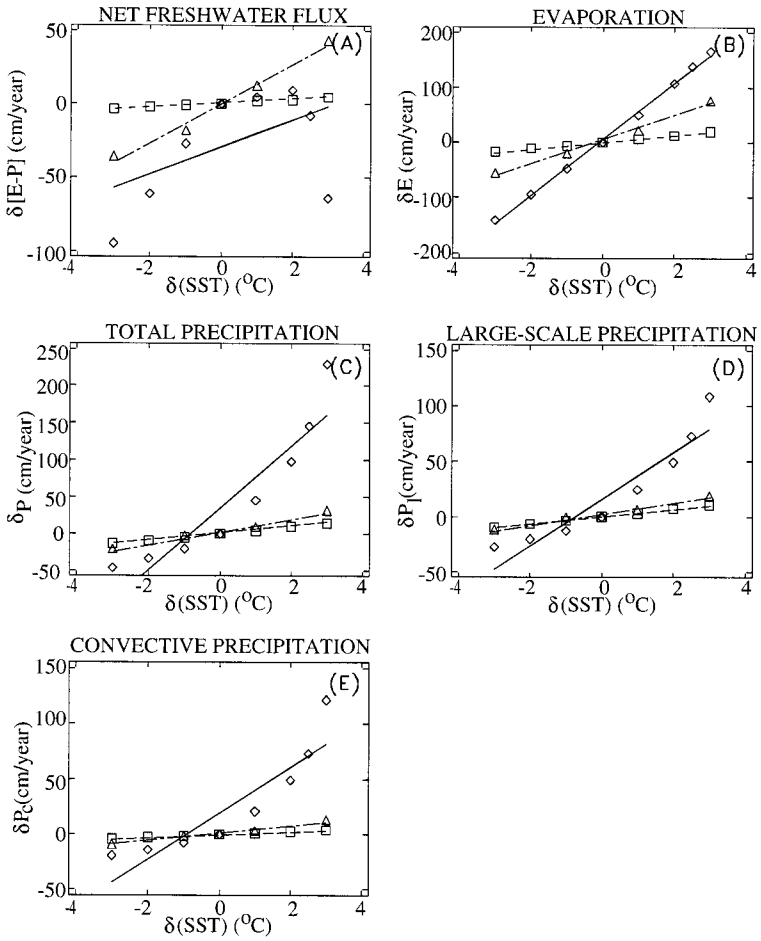

FIG. 7. The same as in Fig. 6 for the TSjan (diamonds, solid line), MMjul (triangle, dash–dot), and GBjul SST (squares, dash) perturbations.

flux parameterization for a time-dependent ocean model should reflect the sensitivity of the air–sea heat flux to changes in the SST, as well as to the spatial size of the SST perturbation (see Bretherton 1982; Marotzke 1994). Additional complications as compared with (3) are the different atmospheric response near continents (Seager et al. 1995), and at different latitudes and seasons (see previous section).

In an effort to improve upon Haney's formulation, Willebrand (1993) and Rahmstorf and Willebrand (1995) suggested the following parameterization of the dependence of the air–sea heat flux on the spatial scale of SST perturbations

$$Q = \alpha(T^* - T_o) + \mu\nabla^2(T^* - T_o). \qquad (4)$$

In this expression the magnitude of the second term depends on the spatial scale of SST perturbation. The spatial Fourier transform of this expression is

$$\hat{Q}(k, l, t) = \left[\alpha + \left(\frac{2\pi}{\lambda}\right)^{-2}\mu\right](\hat{T}^* - \hat{T}_o), \qquad (5)$$

where the hat denotes Fourier transform and $\lambda = \sqrt{k^2 + l^2}$ is the wavelength. Following Marotzke (1994), we can analyze the restoring time as a function of the wavelength, and compare to our results, assuming that the size of the SST perturbation is equal to half the corresponding wavelength. The comparison given in Fig. 8 shows that the parameterization (4) of Rahmstorf and Willebrand (1995) is not too far from our AGCM results, although it tends to somewhat overestimate the sensitivity of the restoring time to the spatial scale of SST perturbation [the figure uses the values $\mu = 8 \times 10^{12}$ W K^{-1} and $\alpha = 3$ W m^{-2} K^{-1} suggested in Rahmstorf and Willebrand (1995)]. Fitting (4) to our AGCM results gives $\mu = 28.3 \times 10^{12}$ W K^{-1} and $\alpha = 2.8$ W m^{-2} K^{-1}.

Several works during the last few years demonstrated that the stability and variability of the THC in ocean GCMs under mixed boundary conditions strongly depend on the value of the temperature restoring time and more generally on the heat-flux formulation (Zhang et al. 1993; Power and Kleeman 1994; Rahmstorf and Willebrand 1995; Mikolajewicz and Maier-Reimer 1994). In particular, weak temperature forcing (a large restoring

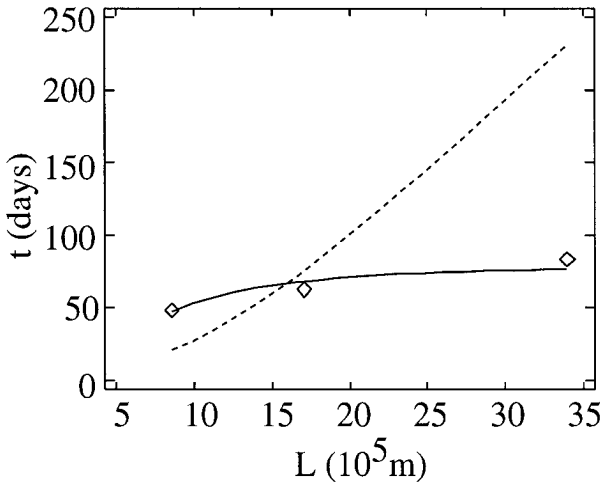

FIG. 8. The dependence of the atmospheric restoring time of SST perturbations on the spatial scale (east–west length) of the SST perturbations. The restoring times for the MSjan, MMjan, and MLjan SST perturbations are shown by the diamonds. The solid line is the least squares best fit to the Rahmstorf and Willebrand (1995) formula (4), which gives $\mu = 28.3 \times 10^{12}$ W K^{-1} and $\alpha = 2.8$ W M^{-2} K^{-1}. The dash line corresponds to the same formula (4) with the values $\mu = 8 \times 10^{12}$ W K^{-1} and $\alpha = 3$ W m^{-2} K^{-1} suggested by Rahmstorf and Willebrand.

time) results in a more stable THC. Stronger temperature restoring can cause the collapse of the North Atlantic overturning circulation and the ''polar halocline catastrophe.'' Power and Kleeman (1993) found that a coarse-grid global version of the GFDL GCM is unstable under mixed boundary conditions for restoring times of less than 25 days and stable for longer restoring times. Zhang et al. (1993) demonstrated that their planetary-geostrophic OGCM is unstable for restoring times less then 200 days and stable when the restoring time is longer then 250 days. The depth of the upper layer was 50 m in Power and Kleeman (1993) and 46 m in Zhang et al. (1993), both comparable to our assumed depth of 50 m.

Our estimates for the restoring times for nonglobal perturbations vary between 44 and 91 days depending on the spatial scale, position, and season of the perturbation (Table 3). Such restoring times will lead to a stable solution in Power and Kleeman (1993) OGCM but to an unstable solution in Zhang et al. (1993) OGCM. This seems to support the speculation of Tziperman et al. (1994) that their realistic OGCM solution is near the stability transition point. In addition, Weaver et al. (1991) and Tziperman et al. (1994) also showed that the strength of the salinity forcing also plays an important role in determining the stability of ocean GCMs, which may explain some of the discrepancies between Power and Kleeman (1993) and Zhang et al. (1993).

6. The model dependence of our results

An obvious concern regarding the atmospheric response to SST anomalies calculated in the preceding sections is their possible model dependence (Frankingoul 1985b). To put our results in perspective and examine their possible model dependence, we compare the sensitivity of the CCM1 AGCM used in this study to the sensitivity of 19 AGCMs to global perturbations examined in Randall et al. (1992) (see also Cess et al. 1990). For this purpose, we performed two perpetual July simulations with ± 2 K global SST perturbations. Table 5 demonstrates that the sensitivity of CCM1 is quite similar to that of other AGCMs, thus enhancing the significance of our results also for the nonglobal perturbations.

TABLE 5. A comparison of our results with other AGCMs for a global SST perturbation. The response of the different components of the surface energy budget when SST is globally increased by 4 K (calculated as a difference between +2 K and −2 K global SST anomalous experiments). The results of the GBjul experiment are compared with the results from various AGCMs from Randall et al. (1992). All units are W m^{-2}.

Variable	CCM1 +2 minus −2	Other models +2 minus −2			
		min	max	mean	std
LE	−15.84	−7.76	−19.98	−12.15	3.17
H	2.39	−0.07	3.85	1.77	0.96
$[SW]_s$	0.15	−8.25	4.00	0.39	2.55
$[LW]_s$	5.22	7.85	0.07	3.27	1.98
Q	−8.38	−3.54	−11.17	−7.61	2.55

Since the turbulent air–sea heat fluxes dominate the atmospheric restoring of SST perturbation, the parameterization of the atmospheric boundary layer is most crucial for getting the atmospheric response correctly in AGCMs. Surface fluxes are calculated in our AGCMs using variables averaged over the lowest atmospheric layer, which is about 1 km thick. The bulk formulas, on the other hand, require the near-surface atmospheric temperature (often at a 10-m height). To interpolate the lowest-level atmospheric model quantities to the near-surface level, an explicit planetary boundary layer model should be used. But this is not done in most GCMs because of computational cost considerations. One particular consequence of the resulting simple representation of the atmospheric boundary layer is the possibly biased dependence of the lower atmospheric lapse rate on the SST. In the case of a local equilibrium between the atmospheric surface temperature and the SST (i.e., the weak advection limit) the near-surface atmospheric temperature follows the SST changes so that the near-surface lapse rate is almost constant with respect to SST changes (Seager et al. 1995). In the CCM1 model employed in our study, we find that the atmospheric temperature, and therefore also the near-surface lapse rate, change with the SST. This might be a result of using the temperature at the lowest atmospheric model level instead of the actual near-surface atmospheric temperature in the bulk formulas. The changing lapse rate induces an additional sensitivity of the air–sea fluxes to the SST, which may not exist in the real system where the lapse rate is less sensitive to the SST. Therefore, our

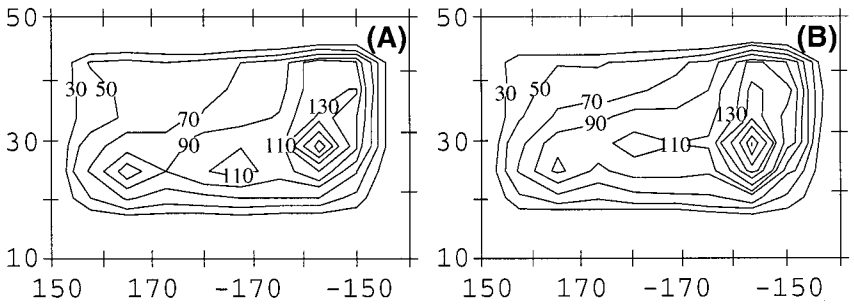

FIG. 9. The spatial variations of the restoring times (in days) for the (A) +1MLjan and (B) +2MLjan SST perturbations.

results may reflect an oversensitivity of the surface fluxes in CCM1 to the SST and our estimates of the atmospheric restoring time may thus be lower bounds.

The linearity of the air–sea heat flux anomaly response to SST perturbations is very robust in our experiments. A verification of this finding based on the analysis of observations is not feasible because of the difficulties in directly measuring air–sea fluxes, and because it is hard to separate the effect of SST perturbations on the air–sea fluxes from other effects. The sensitivity of the air–sea fluxes to SST changes in our experiments mainly depends on the response of the air–sea temperature difference. Because the atmospheric temperature in the lower troposphere responds linearly to SST perturbations in our model experiments, so does the air–sea heat flux. Kushnir (1994) showed that the air temperature fluctuation in the North Atlantic during this century mostly follow the SST fluctuations with some differences, which may be attributed to measurement errors. Allen and Davey (1993) did not find any significant nonlinearities in their analysis of the air–sea heat flux response to tropical SST perturbations. Hence, the existing climate data do not contradict our conclusion concerning the linear relation between SST perturbations and the air–sea flux in the region of the SST anomaly.

A relevant model study that may be used to examine the linearity issue is that of Power et al. (1995), who analyzed the response of the restoring coefficient (inverse restoring time) in an AGCM to two SST anomaly amplitudes in the North Atlantic. In distinction to our experiments, their SST anomaly was not uniform and was situated over the whole North Atlantic including the near-coast regions. They find that the spatial extremum of the locally calculated restoring coefficient intensifies with the increase of SST perturbation. This led them to conclude that the atmospheric response to SST perturbations is nonlinear. Nevertheless, the averaged changes to the restoring coefficient over their region of perturbation seem to be small, indicating a nearly linear atmospheric response, with a restoring time between 1.5 and 2 months. Following Power et al. (1995), we compare the spatial structure of the restoring times for MLjan perturbations of +1°C and +2°C. Figure 9 demonstrates that while the restoring time varies over the perturbation area, it is almost unchanged in these two experiments, which means that our atmospheric model responds linearly both locally and in the spatially averaged response. Lau and Nath (1990) described a nonlinear response of the air–sea fluxes to SST perturbation, but they analyzed the transient, not long-term averaged atmospheric response that is relevant to decadal climate variability. Kushnir and Lau (1992) found nonlinear effects in the the atmospheric response to large-area SST anomalies in the North Atlantic. A direct comparison with our results is difficult, however, due to the complex spatial structure of their anomalies and the different analysis procedure.

We conclude that the linearity of the air–sea fluxes response to SST anomalies is probably a robust result. The specific values for the restoring times are similar to those seen in other coarse AGCMs, yet less certain due to the poor boundary layer parameterization in such coarse models.

7. Conclusions

Numerical experiments with the NCAR CCM1 atmospheric general circulation model demonstrate a linear response of air–sea heat fluxes to SST perturbations for a wide range of perturbation amplitudes. The atmospheric restoring time of SST perturbations calculated for a 50-m mixed layer depth vary from 1.5 to 3 months for nonglobal perturbations and is about 1.5 yr for a global perturbation. As anticipated, the larger the spatial scale of perturbation, the longer the restoring time. On the other hand, the latent heat flux, and not the longwave radiation, is the most sensitive component of the heat-flux response even for global SST perturbations, in contradiction to the anticipation of previous studies.

We find only a weak dependence of the atmospheric restoring time on the latitude of SST perturbation. The seasonal dependence is stronger, with the restoring time shorter in winter than in summer. The air–sea freshwater flux was found to strongly depend on the amplitude of SST perturbations, unlike in common boundary condition formulations in ocean-only models.

The implications of our findings to the boundary condition formulation of ocean-only models were examined

here in detail. It has been shown by several previous studies that the stability and variability behaviors of ocean-only models is very sensitive to the atmospheric feedbacks examined here in detail. We hope, therefore, that the quantitative analysis of the atmospheric feedbacks offered here will advance our ability to model the climate system and help formulate more accurate ocean-only models for climate stability and variability studies.

Acknowledgments. We thank two anonymous reviewers for their constructive comments. We thank the National Center for Atmospheric Research for providing us the CCM1 code. Partial funding for IR is provided by a fellowship from the Feinberg Graduate School, Weizmann Institute of Science. This study was partially funded by the Israeli Science Foundation.

APPENDIX

Air–Sea Flux Parameterization in CCM1

The model used in this study is an R15, 12-level version of the National Center for Atmospheric Research (NCAR) Climate Community Model (CCM1) (Williamson et al. 1987). The heat flux into the ocean, Q, is calculated in the model from the surface heat budget equation

$$Q = [\mathrm{LW}]_s + [\mathrm{SW}]_s^{\downarrow} + H + [\mathrm{LE}], \qquad \text{(A1)}$$

where [LW] and $[\mathrm{SW}]^{\downarrow}$ are the net downward longwave and upward shortwave (solar) radiative fluxes, E is the rate of evaporation, and H and $[\mathrm{LE}] = -\mathrm{LE}$ are the vertical fluxes of the sensible and latent heat at the surface, where $L = 2.5014 \times 10^6$ J kg^{-1} is the latent heat of evaporation. The subscript s denotes variables at the sea surface.

The net LW flux $[\mathrm{LW}]_s$ is the difference between the downward LW radiation from the atmosphere and clouds, $[\mathrm{LW}]_s^{\downarrow}$, and the upward emission from the sea surface, that is proportional to the fourth power of the sea surface temperature, T_s,

$$[\mathrm{LW}]_s = [\mathrm{LW}]_s^{\downarrow} - \sigma_B T_s^4. \qquad \text{(A2)}$$

Here, $\sigma_B = 5.6701$ W m^{-2} K^{-4} is the Stefan–Boltzmann constant. The downward LW flux $[\mathrm{LW}]_s^{\downarrow}$ depends mainly on the fraction of cloud cover, on the height of the lower cloud boundary, on the fourth power of the atmospheric temperature, and on the atmospheric humidity (at all model levels if cloud cover is less than 100% and at levels bellow the clouds otherwise). The emissivity of atmospheric gases (CO_2, O_3, and H_2O), as well as radiative properties of clouds are specified. The SW radiation depends on the atmospheric humidity and cloud cover, as well as on the specified parameters such as O_3 and CO_2 mixing ratios, clouds, and ocean albedo.

The sensible air–sea heat flux and evaporation are calculated by the usual bulk formulas

$$H = c_p \rho_h C_H |\mathbf{V}|(\theta_h - T_s), \qquad \text{(A3)}$$

$$E = \rho_h C_H |\mathbf{V}|[q_m(T_s, p_s) - q_h]. \qquad \text{(A4)}$$

Here, c_p is the specific heat capacity of air at constant pressure (including the humidity effect); ρ is the air density; C_H is the drag coefficient, which is a function of the bulk Richardson number; $|\mathbf{V}|$ is the velocity magnitude; q and θ are the atmospheric humidity and potential temperature, correspondingly; and $q_m(T, p)$ is the saturation humidity at a temperature T and pressure p. The subscript h denotes the first vertical atmospheric grid level above the earth surface. The velocity is written as $|\mathbf{V}| = \sqrt{|\mathbf{V}_h| + |\mathbf{V}_c|}$, where $|\mathbf{V}_c|$ is a convective component taken into account if the lowest level of the atmosphere is unstable.

The air–sea freshwater flux is the difference of local evaporation E and precipitation P, where precipitation is the sum of the large-scale stable and convective precipitations. Precipitation takes place if the moisture at some model level is supersaturated. If the lapse rate is unstable, the temperature and specific humidity are modified to make the layer stable and saturated (moist adiabatic adjustment); if the lapse rate is stable, the temperature and moisture adjust simultaneously to make the layer just saturated. Condensed moisture precipitates immediately without evaporation in layers bellow the condensation level.

Clouds affect both the solar (downward) and terrestrial (upward) radiative fluxes. All the radiative characteristics of clouds are specified; the longwave flux clouds are assumed to behave as blackbodies. In the model, clouds are divided into convective and nonconvective, and are parameterized separately. The convective cloudiness is formed in layers effected by convective adjustment, the total convective cloud cover column is specified as 30%. Nonconvective clouds are formed where stable condensation takes place, if the total rate of precipitation at some level is greater than zero, nonconvective clouds are formed with a fractional cloud cover of 95%; the total cloud cover is calculated assuming a random overlap of nonconvective clouds at different levels.

REFERENCES

Allen, M. R., and M. K. Davey, 1993: Empirical parameterization of tropical ocean–atmosphere coupling: The inverse Gill problem. *J. Climate,* **6,** 509–530.

Blackmon, M. L., 1985: Sensitivity of January climate response to the position of Pacific sea-surface temperature anomalies. *Coupled Ocean–Atmosphere Models,* J. C. J. Nihoul, Ed., Elsevier, 19–28.

Bretherton, F. P., 1982: Ocean climate modeling. *Progress in Oceanography,* Vol. 11, Pergamon Press, 93–129.

Bryan, F., 1986: High-latitude salinity effects and interhemispheric thermohaline circulation. *Nature,* **323**(25), 301–304.

Cai, W., and S. J. Godfrey, 1995: Surface heat flux parameterization and the variability of thermohaline circulation. *J. Geophys. Res.,* **100**(C6), 10 679–10 692.

Capotondi, A., and R. Saravanan, 1996: Sensitivity of the thermohaline circulation to surface buoyancy forcing in a two-dimensional ocean model. *J. Phys. Oceanogr.,* **26,** 1039–1058.

Cess, R. D., and Coauthors, 1990: Intercomparison and interpretation of climate feedback processes in 19 atmospheric general circulation models. *J. Geophys. Res.*, **95,** 16 601–16 615.

Chen, F., and M. Ghil, 1995: Interdecadal variability of the thermohaline circulation and high-latitude surface fluxes. *J. Phys. Oceanogr.*, **25,** 2547–2568.

Chervin, R. M., J. E. Kutzbach, D. D. Houghton, and R. G. Gallimore, 1980: Response of the NCAR general circulation model to prescribed changes in ocean surface temperature. Part I: Midlatitude and subtropical changes. *J. Atmos. Sci.*, **37,** 308–332.

Delworth, T., S. Manabe, and R. J. Stouffer, 1993: Interdecadal variations of the thermohaline circulation in a coupled ocean–atmosphere model. *J. Climate*, **6,** 1993–2011.

Frankingoul, C., 1985a: Multivariate analysis of sensitivity studies with atmospheric GCMs. *Coupled Atmosphere–Ocean Models*, J. C. J. Nihoul, Ed., Elsevier Oceanography Series Vol. 40, Elsevier, 199–209.

——, 1985b: Sea surface temperature anomalies, planetary waves and air-sea feedback in the middle latitude. *Rev. Geophys.*, **23,** 357–390.

Gill, A. E., 1982: *Atmosphere–Ocean Dynamics*. Academic Press, 662 pp.

Haney, R. L., 1971: Surface thermal boundary conditions for the ocean model. *J. Phys. Oceanogr.*, **1,** 241–248.

Hoskins, B. J., and D. J. Karoly, 1981: The steady linear response of a spherical atmosphere to thermal and orographic forcing. *J. Atmos. Sci.*, **38,** 1179–1196.

Kleeman, R., and S. Power, 1995: A simple atmospheric model of surface heat flux for use in ocean modeling studies. *J. Phys. Oceanogr.*, **25,** 92–105.

Kushnir, Y., 1994: Interdecadal variations in North Atlantic Sea surface temperature and associated atmospheric conditions. *J. Climate*, **7,** 141–157.

——, and N.-C. Lau, 1992: The general circulation model response to a North Pacific SST anomaly: Dependence on time scale and pattern polarity. *J. Climate*, **5,** 271–283.

Kutzbach, J. E., R. M. Chervin, and D. D. Houghton, 1977: Response of the NCAR general circulation model to the prescribed changes in ocean surface temperature. Part I: Mid-latitude changes. *J. Atmos. Sci.*, **34,** 1200–1213.

Lau, N.-C., and M. J. Nath, 1990: A general circulation model study of the atmospheric response to extratropical SST anomalies observed in 1950–79. *J. Climate*, **3,** 969–989.

Maier-Reimer, E., U. Mikolajewicz, and K. Hasselmann, 1993: Mean circulation of the Hamburg LSG OGCM and its sensitivity to the thermohaline surface forcing. *J. Phys. Oceanogr.*, **23,** 731–757.

Manabe, S., R. J. Stouffer, M. J. Spelman, and K. Bryan, 1991: Transient responses of a coupled ocean–atmosphere model to graduate changes of atmospheric CO_2 Part I: Annual mean response. *J. Climate*, **4,** 785–818.

Marotzke, J., 1989: Instabilities and multiple steady states of the thermohaline circulation. *Oceanic Circulation Models: Combining Data and Dynamics*, D. L. T. Anderson and J. Willebrand, Eds., NATO ASI Series, Vol. C284, Kluwer, 501–511.

——, 1994: Ocean models in climate problems. *Ocean Processes in Climate Dynamics: Global and Mediterranean Examples*, P. Malanotte-Rizzoli and A. R. Robinson, Eds., Kluwer Academic Publishers, 79–109.

Mikolajewicz, U., and E. Maier-Reimer, 1990: Internal secular variability in an ocean general circulation model. *Climate Dyn.*, **4,** 145–156.

——, and ——, 1994: Mixed boundary conditions in ocean general circulation models and their influence on the stability of the model's conveyor belt. *J. Geophys. Res.*, **99,** 22 633–22 644.

Moore, A. M., and C. J. C. Reason, 1993: The response of a global general circulation model to climatological surface boundary conditions for temperature and salinity. *J. Phys. Oceanogr.*, **23,** 300–328.

Nakamura, M., P. H. Stone, and J. Marotzke, 1994: Destabilization of the thermohaline circulation by atmospheric eddy transport. *J. Climate*, **7,** 1870–1882.

Peixoto, J. P., and A. H. Oort, 1992: *Physics of Climate*. American Institute of Physics, 520 pp.

Phillips, T. J., and A. J. Semptner Jr., 1984: The seasonal response of the Held–Suarez climate model to prescribed ocean temperature anomalies. Part I: Results of decadal integrations. *J. Atmos. Sci.*, **41,** 2605–2619.

Power, S. B., and R. Kleeman, 1993: Multiple equilibria in a global OGCM. *J. Phys. Oceanogr.*, **23,** 1670–1681.

——, and ——, 1994: Surface heat flux parameterization and the response of ocean general circulation models to high-latitude freshening. *Tellus*, **46,** 86–95.

——, A. M. Moore, D. A. Post, N. R. Smith, and R. Kleeman, 1994: Stability of North Atlantic deep water formation in a global ocean general circulation model. *J. Phys. Oceanogr.*, **24,** 904–916.

——, R. Kleeman, R. Colman, and B. McAvaney, 1995: Modeling the surface heat flux response to long-lived SST anomalies in the North Atlantic. *J. Climate*, **8,** 2161–2180.

Rahmstorf, S., and J. Willebrand, 1995: The role of temperature feedback in stabilizing the thermohaline circulation. *J. Phys. Oceanogr.*, **25,** 787–805.

Randall, D. A., and Coauthors, 1992: Intercomparison and interpretation of surface energy fluxes in atmospheric general circulation models. *J. Geophys. Res.*, **97**(D4), 3711–3724.

Rivin, I., and E. Tziperman, 1997: Linear versus self-sustained interdecadal thermohaline variability in a coupled box model. *J. Phys. Oceanogr.*, **27,** 1216–1232.

Schopf, P. S., 1983: On equatorial waves and El Niño. II. Effects of air–sea thermal coupling *J. Phys. Oceanogr.*, **13,** 1878–1893.

Seager, R., Y. Kushnir, and M. Cane, 1995: An advective atmospheric mixed layer model for ocean modeling purposes: Global simulation of surface heat fluxes. *J. Climate*, **8,** 1951–1064.

Tziperman, E., R. Toggweiler, Y. Feliks, and K. Bryan, 1994: Instability of the thermohaline circulation with boundary conditions: Is it really a problem for realistic models? *J. Phys. Oceanogr.*, **24,** 217–232.

Washington, W. M., and J. Meehl, 1989: Climate sensitivity due to increased CO_2: Experiments with a coupled atmosphere and ocean general circulation model. *Climate Dyn.*, **4,** 1–38.

Weaver, A. J., and T. M. C. Hughes, 1994: Rapid interglacial climate fluctuations driven by North Atlantic Ocean circulation. *Nature*, **367,** 447–450.

——, E. S. Sarachik, and J. Marotzke, 1991: Freshwater flux forcing of decadal and interdecadal oceanic variability. *Nature*, **353,** 836–838.

Webster, P. J., 1981: Mechanisms determining the atmospheric response to sea surface temperature anomalies. *J. Atmos. Sci.*, **38,** 554–571.

Weisse, R., U. Mikolajewicz, and E. Maier-Reimer, 1994: Decadal variability of the North Atlantic in an ocean general circulation model. *J. Geophys. Res.*, **99,** 12 411–12 422.

Willebrand, J., 1993: Forcing the ocean with heat and freshwater fluxes. *Energy and Water Cycles in the Climate System*, E. Raschke, Ed., Springer-Verlag, 215–233.

Williamson, D. L., J. T. Kiehl, V. Ramanathan, R. E. Dickinson, and J. J. Hack, 1987: Description of NCAR Community Climate Model (CCM1). NCAR Tech. Note NCAR/TN285+STR, 112 pp. [Available from National Center for Atmospheric Research, P.O. Box 3000, Boulder, CO 80307.]

Winton, M., and E. S. Sarachik, 1993: Thermohaline oscillations induced by strong salinity forcing of ocean general circulation models. *J. Phys. Oceanogr.*, **23,** 1389–1410.

Yin, F. L., and E. S. Sarachik, 1995: Interdecadal thermohaline oscillations in a sector ocean general circulation model: Advective and convective processes. *J. Phys. Oceanogr.*, **25,** 2465–2484.

Zhang, S., R. J. Greatbatch, and C. A. Lin, 1993: A reexamination of the polar halocline catastrophe and implications for coupled ocean–atmosphere modeling. *J. Phys. Oceanogr.*, **23,** 287–299.